Flat electron beam sources for DLA accelerators

A. Ody, P. Musumeci, J. Maxson, D. Cesar

UCLA Department of Physics and Astronomy, 475 Portola Plaza, Los Angeles, CA, 90095

R. J. England, K. P. Wootton

SLAC National Accelerator Laboratory, 2575 Sand Hill Rd, Menlo Park, CA, 94025

Abstract

In this paper we discuss the application of the flat beam transform to generate beams suitable for injection into slab-symmetric dielectric laser-driven accelerators (DLAs). A study of the focusing requirements to keep the particles within the tight apertures characterizing these accelerators shows the benefits of employing ultralow beam emittances. The slab geometry of the many dielectric accelerating structures strongly favors the use of flat beams with large ratio between vertical and horizontal emittances. We employ particle tracking simulations to study the application of the flat beam transform for two injector designs, a DC non relativistic photogun and a 1.6 cell S-band RF photoinjector, obtaining in both cases emittance ratios between the horizontal and vertical plane in excess of 100 in agreement with simple analytical estimates. The 4 MeV RF photoinjector study-case can be directly applied to the UCLA Pegasus beamline and shows normalized emittances down to <3 nm in the vertical dimension for beam charges up to 20 fC, enabling a two-stage DLA experiment.

1. Introduction

Dielectric laser accelerators (DLA) hold the promise of future miniaturized particle accelerators. High gradient acceleration in laser-driven dielectric structures has been successfully demonstrated in the last few years [1, 2] and is the subject of intense research activities [3]. One aspect of this research that immediately captures the attention is the inadequateness of conventional electron sources to satisfy the tight beam requirements for DLAs. Apertures smaller than the laser wavelength and angular acceptances in the sub-mrad range coupled with electron bunch charges in the fC range and repetition rates up to MHz demand no less than a revolution in the methods used to generate, diagnose and manipulate electron beams.

Current candidates for electrons sources for DLA are tip-based and flat photocathode electron sources. Recent results of using photoactivated tips in time-resolved electron microscopes have demonstrated outstanding transverse coherence and 100 fs bunch duration when running with very few (< 10) electrons per pulse regime ([4, 5]). Flat photocathodes have a significant advantage for beam charges up to the pC range and have recently demonstrated < 20 nm emittances [6].

The detailed beam parameters for an ideal electron source for DLA obviously are

This material is based upon work supported by the U.S. Department of Energy, Office of Science, under Contract No. DE-AC02-76SF00515.

Parameter	Desired Capability	Unique DLA Features
Electron energy	10-20 MeV	Single-wafer design with GV/m gradient
Useful dose	1 Gray/sec	2000 e- per bunch; 2 MHz rep rate
Treatment volume	5-10 cm^3	Directed (vs. omnidirectional) beam and on-chip deflection to scan tumor-area
Small footprint	$\sim$ 1 cm $\times$ 10 cm	2 μm wavelength optical scale device with 2 cm active linac length
Wall plug power	$<$ 100 W	2.9 % wall-plug to electron efficiency

Table 1: Electron beam parameters for DLA medical applications

strongly dependent on the final application of the accelerator. For the sake of discussion, we can broadly separate electron beam applications in i) coherent radiation generation for which the key parameter is the peak beam current and therefore the number of particles in a single bunch and ii) incoherent radiation or direct electron beam applications where the relevant quantity is the average number of particles per second. Any attempt to find out baseline requirements for the electron source should start from the latter case including, for example, electron beam drivers for bremsstrahlung, inverse compton scattering or spontaneous undulator radiation X-ray sources. In this case it is possible to neglect collective effects as the numbers of electrons per bunch can be kept relatively low and high average currents can be simply achieved by increasing the repetition rate of the accelerator. On the other hand, coherent radiation generation applications will require obtaining comparable (or higher) beam brightness with much larger charge per bunch with the potential of collective effects severely affecting the beam quality, thus imposing additional challenges on the source development.

Looking at an example parameter spreadsheet for medical applications of DLA, typical average currents required are in the order of few mA. Assuming a repetition rate of 100 MHz this current corresponds to 10 fC charge per pulse. Incidentally, these beam charges are ideal from the optical power to electric energy efficiency conversion perspective, as the DLA accelerator will be optimally loaded [18]. A more optimistic estimate of DLA medical applications [3] requirements calls for 2000 electron per pulse (see Table 1). Unfortunately even at these very low charge levels nanotip sources have not yet demonstrated preservation of very low emittances and short pulse durations.

Even though it is conceivable that future progress in nano-tip sources (control of the emission area, shaping of the laser field, nanotip lenses, etc.) would lead to significant improvements in the performance of these sources, the present paper is devoted to evaluating flat photocathode-based sources as a more viable near-term solution for real-world applications of DLA accelerators. Assuming 10-20 fC as the ideal target charge per bunch, we will discuss the optimal source design to fit the tight transverse phase

space DLA requirements.

A path to answer this question comes from the observation that all actively researched DLA structures use a slab geometry so that the requirements in the small gap dimension (arbitrarily here set to y or vertical) are much tighter than in the other dimension (x or horizontal). More than a decade ago, it was pointed out [7] that starting from a magnetized cathode a linear transformation based on a skew quadrupole triplet can be used to remove the angular momentum on the beam induced by the magnetic field and obtain large asymmetry in the phase space areas occupied by the beam in the two transverse dimensions. This scheme – commonly referred to as the flat beam transform (FBT) – has been demonstrated in a series of experiments at Fermilab[8, 9] in the framework of the development of a source for a high energy physics linear collider. In this paper, expanding the analysis in [10] we analyze the applicability of this technique to the challenge posed by the generation of a beam suitable for DLA which demands ultralow vertical emittances but could tolerate much larger (up to 100 times) horizontal emittances.

Depending on what energy one designs the handshake between the source and the laser-driven DLA accelerating structures the technology for the electron source can greatly differ. We will investigate here two cases (100 kV and 4 MeV) as these energies fall well within the range of widely available DC photogun and RF photogun sources. These examples serve to illustrate the physics challenges in each regime. Further, the study for 4 MeV can be immediately applied to the Pegasus ACHIP experiments [11]. Nevertheless, the approach is valid in general and can be scaled to other more complicated gun designs (including TOPGUN [12], hybrid guns [13], 1.4 cell guns [14] and so on) which are currently under study by various groups at SLAC, UCLA, etc.

The paper proceeds as follows. We start with a discussion of the focusing requirements in DLAs in order to clarify where the limits on the required beam emittance come from. We then review the basic theory and formulas of the flat beam transform technique pointing out how in the very low charge limit, ultralow emittances – which are independent on the laser spot size on the cathode – can be obtained in the small dimension. We then analyze in detail realistic cases for a 100 keV DC photogun and a 4 MeV RF photoinjector beamline including the effects of space charge. The conclusions include the discussion of a possible two stage DLA experiment enabled by the few nm normalized emittance obtained with the FBT.

2. Focusing Requirements for DLA

We consider here the generic focusing requirements in a channel of constant size with a uniform loaded accelerating gradient. We will then evaluate the focusing requirements for different configurations relevant to DLA. We begin with the usual formulation of the envelope equation:

$$\sigma'' + \frac{\gamma'}{(\beta\gamma)^2}\sigma' - \left[\left(\frac{\gamma'}{\beta\gamma}\right)^2 - T^2\right]\sigma - \frac{\epsilon_N^2}{(\beta\gamma)^2\sigma^2} - \frac{K}{\sigma} = 0 \tag{1}$$

where σ is the rms beam envelope, T^2 is the linear focusing term, $K = 2I/(\beta\gamma)^3 I_A$ is the space charge expansion or beam perveance, $I = Q/\tau$ is the electron beam current

Parameter	Description	Units	Value
λ	wavelength	μm	2
σ	beam size	μm	1
T_0	initial kinetic energy	keV	100
T_f	final kinetic energy	MeV	4
Q	bunch charge	fC	4
τ	bunch duration	fs	0.1 - 1000
ϵ_N	normalized emittance	nm rad	2
L	interaction distance	cm	2

Table 2: DLA bunched beam constant gradient parameters

for a charge Q and bunch length τ, and I_A is the Alfven current. Note that in order to derive Eq. 1 the limit of very long cylindrical beams is assumed. This can serve as a first approximation, but it should be mentioned that electron beams accelerating in DLAs will most likely neither be cylindrical nor have a very elongated aspect ratio. For particles that are sub-relativistic, the beam velocity $\beta = v/c$ changes rapidly as the particle accelerates. A tapered accelerator structure is therefore needed in order to continuously match the phase velocity to the particle velocity. If we assume a linearly increasing beam energy (i.e. constant gradient acceleration) with $\gamma(z) = \gamma_0 + \alpha z$ and solve for the external focusing T^2 required to maintain a constant equilibrium envelope size σ then we obtain

$$T^2(z) = \frac{\epsilon_N^2/\sigma^3 + \alpha^2}{(\gamma(z) - 1)^2} + \frac{K(z)}{\sigma^2} \tag{2}$$

This represents the needed variation along z of the focusing field to maintain a constant beam radius. Note that the space charge perveance is also a function of z. To get an order of magnitude sense of the required focusing fields, we consider the example of an optically pre-bunched electron beam with DLA-compatible parameters. The question of how the electrons are generated, pre-bunched, and initially matched in spot size to the accelerating channel are not addressed here. A concept for pre-bunching the particle beam has been presented in Ref. [15] and an optical microbunching scheme using an inverse free electron laser interaction has been demonstrated at relativistic energies [16, 17]. For these example parameters, we plot in Fig. 1 the corresponding tapered linear focusing and space charge perveance terms as a function of beam energy. We see that as the beam accelerates from sub-relativistic to relativistic energy the required normalized focusing term spans 3 orders of magnitude. The microbunch charge of 4 fC used here is consistent in order of magnitude with bunch charge for optimal efficiency for DLA configurations considered in Ref. [18, 19]. Normalized emittances of 2 nm-rad can be obtained from flat photocathodes as we will see below using the flat beam transform technique.

Below we consider the emittance dependence of the focusing force at the two target beam energies (100 keV and 4 MeV) considered later in this paper. In the plots of Fig. 2, the linear focusing of Fig. 1 is plotted as a function of normalized emittance (blue curve). The red curves correspond to a bunch duration of 1 ps, thereby reducing

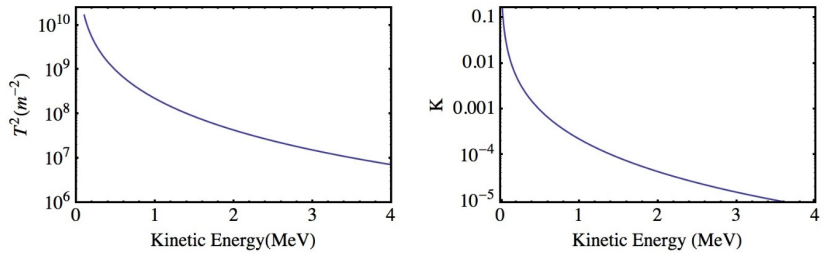

Figure 1: Plots of focusing term and space charge perveance vs. beam energy for the example DLA parameters of Table I for energies from 100 keV to 4 MeV.

the space-charge perveance term in Eq. 2. For reference, we consider three potentially compatible methods of focusing: (i) electrostatic focusing for the low-energy case and (ii) electromagnetic and (iii) magnetostatic focusing for the high-energy case. These are plotted as horizontal dashed lines in Fig. 2. A fourth option (use of a magnetic solenoid) appears less feasible here as the required field strengths exceed what is achievable with known superconducting or permanent magnet designs.

At sub-relativistic energies, electrostatic focusing appears favorable for re-collimation of unbunched beams. The dashed reference line in Fig. 2a was obtained by considering a simple 2-electrode system with cylindrical symmetry separated by a narrow gap. Such a configuration could be implemented in a miniaturized electron source by deposition of conductive electrodes onto an insulating substrate. For example, in a 100 keV electron gun, a second aperture following the anode at a different potential may be introduced as an auxiliary focusing element [20, 21]. The general linear focusing term for a cylindrically symmetric electrostatic lens at sub-relativistic beam energies is given by the relation $T = \sqrt{3}\phi'/[4(\phi - V_0)]$, where ϕ is the axial electrostatic potential and V_0 is the particle energy [22]. Using the formulation of Grivet for the functional form of ϕ for two cylinders of diameter D at potentials V_1 and V_2 separated by a gap of distance S we find an approximate focusing field in the center of the gap

$$T \simeq \frac{\sqrt{3}(V_2 - V_1)}{4S(\frac{V_1+V_2}{2} - V_0)} \tanh w\frac{S}{D} \tag{3}$$

where w=1.318 is a numerical integration constant [23]. We note that for such a lens, a major limiting factor is the dielectric breakdown strength of the insulating material separating the electrodes. For micron-scale thin-film gaps, it has been found that common dielectrics amenable to nanofabrication methods exhibit remarkably high dielectric strengths [24][25]. For fused silica, the thin-film strength has been measured by Szmidt to be χ = 560 MV/m [11]. Using this value in Eq. 3 with a gap S = 1 μm, D = 30 μm, and setting $V_1 = V_0$ and $V_2 = V_0 + \chi S$, we obtain the estimated reference value $T^2 \simeq 1.4 \times 10^9 m^{-2}$ shown by the dashed line in Fig. 2a. In [26][27], a laser-driven focusing scheme based on the dual-grating DLA geometry is proposed with an estimated focusing gradient of B'=0.4 MT/m. Noting that the normalized field is related to the gradient via $B' = T^2\beta\gamma mc/e$, we obtain a corresponding normalized focusing field $T^2 = 1.3 \times 10^7 m^{-2}$ which corresponds to the dashed reference line in Fig. 2b.

A high-gradient permanent magnet quadrupole could provide a solution of intermediate focusing strength (of order $T^2 \sim 10^5$ m^{-2}). In Fig. 2(b) an example value corresponding to this field strength is superimposed on the plot, indicating that with few nm-rad emittance beams, such a solution could provide a means to extend the particle transport over longer distances. Note that these simple estimates assume a continuous focusing force, while in practice focusing elements might alternate with accelerating structures. A more detailed analysis would be needed to assess the effects associated with alternate focusing schemes.

The PMQ case is considered in more detail below in combination with beam parameters for the flat-beam transform scenario. For all these focusing elements a continuous focusing force can not be provided and needs to alternate with regions of acceleration.

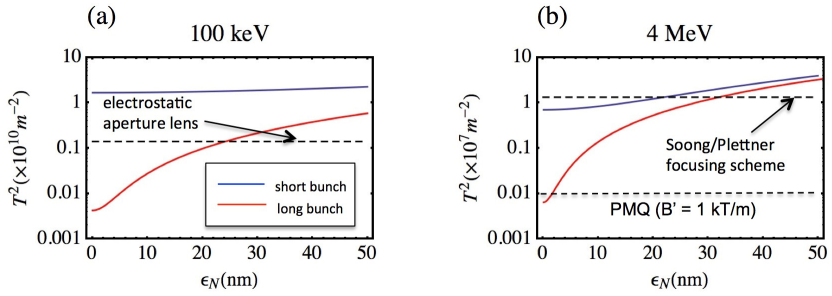

Figure 2: Plots of linear focusing vs. normalized emittance for the example DLA parameters of Table I. For the red curves, the space-charge perveance K is effectively zero, corresponding to a long bunch (non-microbunched) scenario. Dashed lines correspond to estimated focusing for an electrostatic lens (left-hand plot) and the Soong/Pletter laser-driven focusing scenario (right-hand plot).

From these considerations it appears that very low beam emittances should be used whenever possible to ease the extremely high demands on the focusing strength for DLA accelerators.

3. Flat beam transform

It has been shown that an axially symmetric rotating beam can be transformed into a flat beam by an appropriate optical transformation whose result is to split the emittances in the transverse directions. To create a rotating beam, the electron beam is generated by illuminating a cathode within the magnetic field of a solenoid, so that as the particles leave the magnetic field of the solenoid, they gain angular momentum due to fringe field effects. The angular momentum is proportional to the magnetic field amplitude B and to the initial rms spot size at the cathode σ_x:

$$L = \kappa_0 \sigma_x^2 \tag{4}$$

where $\kappa_0 = \frac{eB}{2m_0c}$ where e and m_0 are the electron charge and mass.

The angular momentum can be removed using the so called flat beam transform technique that is a skew quadrupole channel which removes the xy correlation, yielding final emittances given by

$$\epsilon_\pm = \epsilon_{eff} \pm L \tag{5}$$

where $\epsilon_{eff} = \sigma_x \sqrt{\frac{MTE}{m_0 c^2} + (\kappa_0 \sigma_x)^2}$ where MTE is the mean transverse energy due to the photoemission process [28]. For large magnetic field or large spot size on the cathode it is possible to perform a Taylor expansion of this expression and obtain for the limit value of the smaller emittance

$$\epsilon_- \simeq \frac{MTE}{eBc} \tag{6}$$

which is notably independent on the initial spot size. This formula neglects other contributions to the beam emittances coming for example from space charge effects, rf effects and other non linearities.

This is a somewhat surprising result as it means that in this regime the minimum emittance and associated peak 2D brightness are insensitive to the acceleration field on the cathode which usually limits the maximum charge density at the cathode. Furthermore, the minimum value for this emittance is linearly proportional to the MTE, instead of the typical square root dependence, so that application of recent work in minimizing the MTE of photoemission [29, 30] would have a larger impact for flat beam sources.

In Fig. 3 we show the low emittance and the emittance ratio as a function of the magnetic field on the cathode assuming a 50 μm rms spot size and 0.4 eV initial MTE. The simple analytical scaling suggests that emittances approaching few nm can be easily obtained for sub-Tesla field on the cathode. The price to pay for this result is a very large emittance in the other direction. For some applications such as DLA accelerators or also streaked electron diffraction [31] a large degree of asymmetry between the transverse beam emittances is advantageous. For other applications like free-electron lasers or inverse compton scattering [32] it is less clear how to take advantage of strongly asymmetric beams.

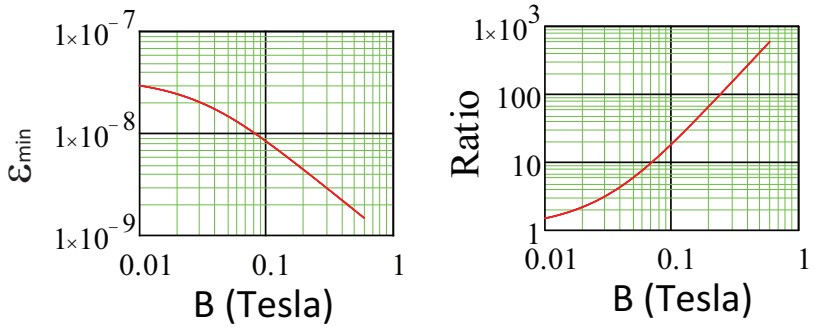

Figure 3: Small emittance and emittance ratio as a function of magnetic field on the cathode. The calculation assumes 0.4 eV MTE and 50 μm rms spot size at the cathode.

In order to split the two transverse emittances, the beam is then transported through a skew quadrupole triplet. Following [33], a 4x4 transformation matrix through 3 unskewed quadrupoles can be shown to be of the form

$$M = \begin{bmatrix} A & 0 \\ 0 & B \end{bmatrix} \tag{7}$$

where A and B are 2x2 block matrices dependent only on the focusing strengths of the quadrupoles and the distances between them. Applying a 45 degrees space rotation to this matrix yields a matrix of the form

$$T = \frac{1}{2}\begin{bmatrix} A_+ & A_- \\ A_- & A_+ \end{bmatrix} \tag{8}$$

with $A\pm = A \pm B$. In order to transform the round magnetized beam to a flat beam, it is then sufficient to satisfy the following equation

$$A_+ S = A_- \tag{9}$$

where S is the symplectic matrix

$$S = \begin{bmatrix} -\alpha & -\beta \\ (1+\alpha^2)/\beta & \alpha \end{bmatrix} \tag{10}$$

and α and β are the Twiss parameters of the input electron beam. The matrix equation 9 above gives 3 equations in terms of the elements of S and the parameters of the quadrupoles. Holding the drift lengths between the quadrupoles (d_2 and d_3) constant, in the thin lens approximation we can then solve for the required focal lengths given incoming values for the Twiss parameters obtaining

$$f_1^{-1} = \pm\sqrt{\frac{-d_2 S_{11} + S_{12} - d_2 d_T S_{21} + d_T S_{22}}{d_2 d_T S_{12}}} \tag{11}$$

$$f_2^{-1} = -\frac{S_{12} + d_T S_{22}}{d_2 d_3 (1 + \frac{S_{12}}{f_1})} \tag{12}$$

$$f_3^{-1} = -\frac{f_1^{-1} + f_2^{-1} + \frac{d_2 S_1 1}{f_1 f_2} + S_{21}}{1 + (d_T f_1^{-1} + d_3 f_2^{-1}) S_{11} + d_2 d_3 f_2^{-1}(S_{21} + f_1^{-1})} \tag{13}$$

$$\tag{14}$$

with $d_T = d_2 + d_3$.

In the rest of the paper we use these initial analytical estimates as input values for a numerical optimization performed with the General Particle Tracer (GPT) code. The optimizer is first used to adjust the magnet currents to take into account thick lens effects and then to include space charge effects. The goal of the optimization is to minimize the remaining correlations between the x and y plane and to maximize the emittance ratio between the two planes.

4. 100 keV DC photogun

The first example we discuss is the 100 keV DC photogun case. This energy represents a reasonable hand-shake energy as 100 keV electron sources are relatively common and the velocity of the particles is a large fraction of the speed of light, easing tapering and resonance structure design. Another advantage is that focusing requirements might be easier to achieve for this energy.

A typical electron beamline is shown in the schematics in Fig. 4. The implementation of the FBT is straightforward and involves adding a solenoid around the cathode to

generate the magnetized beam and 3 skew quadrupoles at the gun exit. When the goal is to obtain sub 5 nm normalized transverse emittance, all aberration sources in the system have to be carefully considered. At non-relativistic electron energies, strong quadrupole lenses can induce a large transverse kick in the electron trajectory sufficient to change its longitudinal velocity resulting in significant coupling between the transverse and longitudinal phase space, with a high impact on the final beam emittance. This kind of aberrations is a strong function of the spot size of the beam in the quadrupoles. In our design a second solenoid is introduced in the beamline to focus the beam at the entrance of the FBT triplet and maintain the spot size (and the angular kicks) small in the system.

In order to further reduce the aberrations, relatively large distances between the quads (30 cm) are employed thus allowing the use of longer focal lengths (i.e. weaker gradient) magnets. A fringe field length of 1 mm is assumed in the simulation. The optimal gradients are sufficiently low that they can easily be obtained with standard electromagnetic quadrupoles. The final beamline parameters are reported in Table 3.

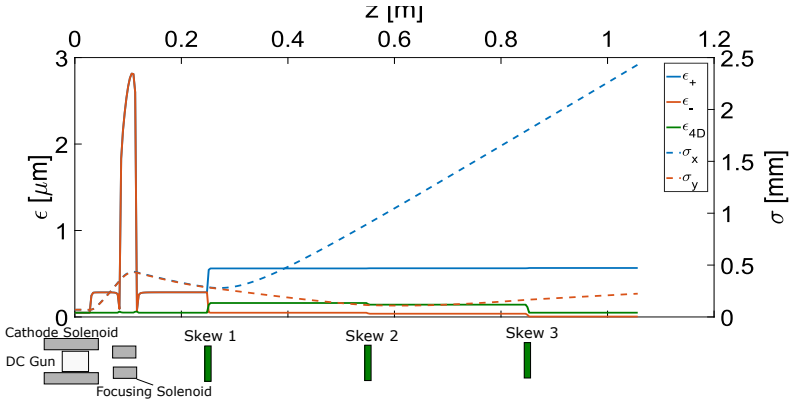

Figure 4: Schematic of 100 keV setup showing the evolution of the transverse emittances and the spot size along the beamline. The 4D emittance is nearly constant along the beamline showing that for these particular configuration the effect of aberrations is negligible.

Emittance ratios in excess of 100 can be obtained with the small emittance reaching few nm level satisfying the demands of the DLA application (see Fig. 4). The footprint of the entire source (DC photogun + quadrupoles) is $\sim$ 0.75 m, the main limit being the aberrations that arise when stronger quadrupole fields are used.

Space charge effects are analyzed, but are found not significant for bunch charges of 20 fC and pulse lengths of 1 ps. They only require a small readjustment in the skew quadrupole values. In practice, the beam-based tuning of the quadrupoles would require the development of 4d phase space diagnostics for very low emittance beams [34].

	Space charge off	Space charge on
Beam energy	100 keV	100 keV
Laser spot on cathode	70 μm	70 μm
Beam charge	0	20 fC
Bunch length	1 ps	1 ps
Magnetc effective length	3 mm	3 mm
Quad spacing	30 cm	30 cm
Quad gradients	(2.11, 0.051, 0.077) T/m	(1.99, 0.028, 0.089) T/m
Emittance ratio	101	82

Table 3: Parameters of FBT for 100 keV gun

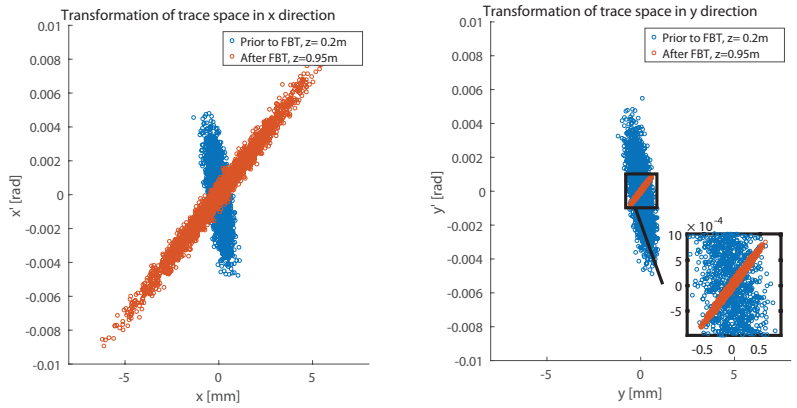

Figure 5: Horizontal and Vertical trace spaces at the beginning and at the end of the skew quadrupole transformation.

5. S-band RF photoinjector

In this section we consider retrofitting the Pegasus beamline to host a flat beam transform section. The Pegasus beamline has set unprecedented records in terms of very low emittance and high brightness beams [6] and is well suited to explore the limits of the techniques discussed in this paper. A schematic picture of the Pegasus beamline showing the location where the flat beam transform can be installed is shown in Fig. 6.

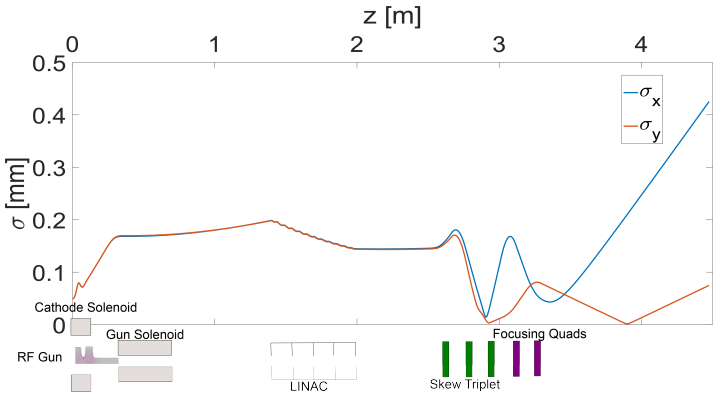

Figure 6: Horizontal and vertical rms spot sizes along the Pegasus beamline for proposed flat beam transform configuration.

In the study of this beamline we add a quadrupole doublet to focus down the beam to a small spot size at the DLA structure entrance after the 3 skew quadrupoles which are used to remove the angular momentum from the beam.

	Space charge off	Space charge on	Theoretical
Energy at gun exit	4 MeV	4 MeV	
Energy at DLA structure	8 MeV	8 MeV	
Laser Spot on Cathode	50 μm	50 μm	
B Field on Cathode	0.1968 T	0.1968 T	
Beam Charge	0 fC	20 fC	
Quad Length	10 cm	10 cm	
Quad Spacing	7.5 cm	7.5 cm	
Quad Gradients	(1.28,-2.92,15.4) T/m	(1.28,-2.92,15.4) T/m	
Focus Quad Gradients	(-3.64,1.98) T/m	(-3.61, 1.98) T/m	
Deviation in x, σ_x	278 μm	210 μm	
Deviation in y, σ_y	1.27 μm	1.37 μm	
High Emittance, ϵ_+	277 nm	277 nm	292 nm
Low Emittance, ϵ_-	2.92 nm	3.01 nm	3.35 nm
Ratio of Emittances	95	92	87

Table 4: Parameters of FBT for S-band photoinjector

GPT optimization is performed to find the quadrupole setting that minimize the y spot size including again the finite effective length (10.4 cm) of the quadrupoles and the space charge effects. The final beam parameters are reported in Table 4, and compared with values we predicted with Eq. 5. Tuning the electron beam energy with the linac will require to retune the currents in the quadrupoles.

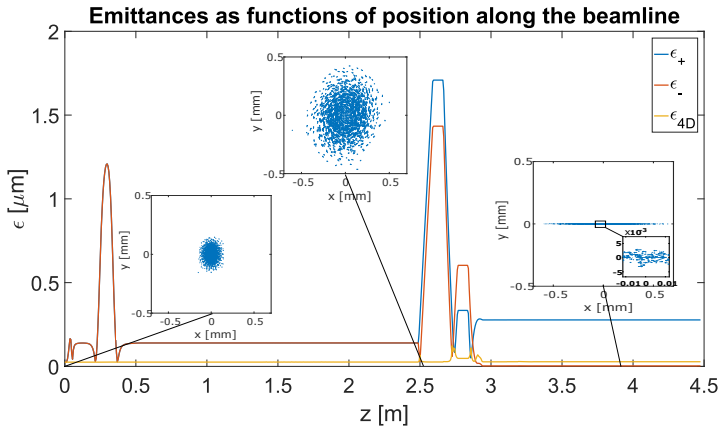

Figure 7: Emittances as a function of distance from the cathode along the relativistic electron beamline. The XY configuration spaces at the entrance (left), before the skew quadrupole channel (middle) and at the focus (right) where the DLA structure will be.

We can follow the evolution of the emittances and the spotsizes along the beamline in Fig. 7. The little blue arrows indicate the transverse velocity of each particles, illustrating how the angular momentum of the beam is removed by the FBT technique. The xy configuration space of the beams at the cathode, at the entrance of the skew quadrupole transform and at the DLA sample are shown in Figure 9.

In this configuration the rms vertical size of the beam at the focus can be smaller than 1.5 μm so that the transmission through a 2 μm-driven DLA could be significantly increased as it will be discussed in the next session.

Simulations with up to 100 fC beam charge were performed finding no particular degradation in the beam parameters. In Fig. 8, the emittance is shown to stay below 5 nm at these levels of charge. The vertical 2D brightness (i.e. Q/ϵ_y) is increased by nearly one order of magnitude with respect to the values currently used at Pegasus for the DLA experiments [34].

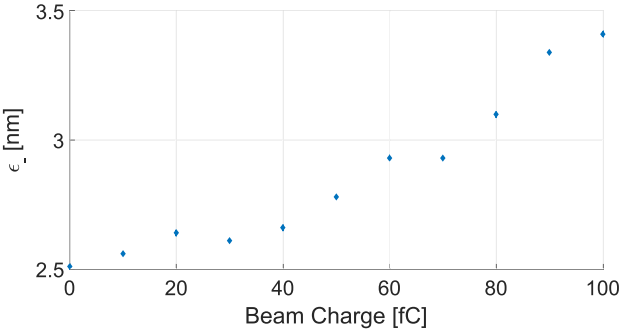

Figure 8: Results of GPT optimization for different beam charges at the cathode. For a 100 fC beam charge an emittance below 5 nm is obtained.

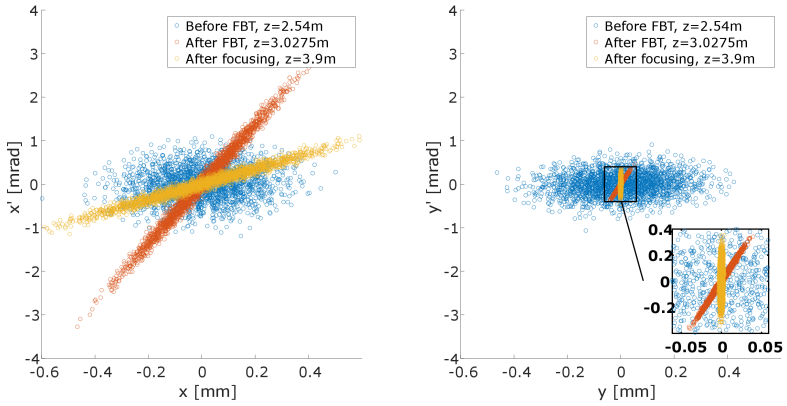

Figure 9: Trace spaces for x and y dimensions. The trace space at the entrance of the DLA structure (after focusing quads) are also shown. The scale of the axes are kept the same to represent the large asymmetry in volume occupied by the beam in the horizontal and vertical dimension. Also note that the final doublet is tune to put the waist at the entrance of the DLA while in the horizontal direction the beam is slightly diverging. In principle one could use a triplet to fully control the beam parameters at the entrance plane of the structure.

6. Two stage DLA experiment at Pegasus

The application of the flat beam transform will generate a beam of unprecedented brightness which could enable two-stage DLA at Pegasus. In this section we study in detail the more concrete example of focusing requirements for a two-stage DLA experiment wherein a long (compared to the laser wavelength) electron bunch is energy modulated in the first stage and then undergoes net acceleration in the second stage, with a drift in between for velocity bunching. We consider a target beam energy of 4 MeV which corresponds to the UCLA photoinjector exit energy. This is shown schematically in Fig. 10a below. Two DLA stages of lengths L are separated by an intervening drift of length l.

The longitudinal dispersion for a beam of energy γ_0 in a drift of length l is given by $R_{56} = dz/d\delta = l/\gamma_0^2$. If the energy modulation amplitude is 30 keV (or η=0.008) in the first stage (consistent with recently measured experimental results [35]), for a 4 MeV electron beam and a wavelength of 2 μm, optimal bunching requires a longitudinal shift by $\lambda/4$ and so will occur after a distance $l \simeq \gamma_0^2(\lambda/4\eta) = 2$ mm. The corresponding parameters are listed in the table below, consistent with current experimental parameters at the UCLA facility. The second case (Case 2) corresponds to the proposed flat-beam transform scenario which was discussed in the prior section.

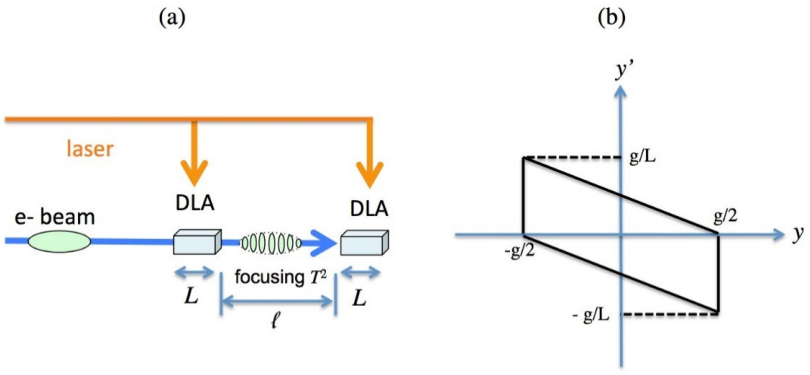

Figure 10: Schematic (a) of a two-stage bunching and net acceleration setup with (b) the acceptance aperture of the first stage DLA entrance in the trace space for a vertical aperture of width g.

Table 5: DLA two stage experiment Example Parameters

Parameter	Description	Units	Case 1	Case 2
λ	wavelength	μm	2	2
g	beam aperture	μm	1	1
U_0	beam energy	MeV	4	4
Q	bunch charge	fC	300	50
τ RMS bunch duration	fs	160	160	
$\epsilon_{Nx,y}$	normalized emittance	nm rad	30	200,2
$\sigma_{x,y}$	RMS spot size	μm	12	200, 1
L	DLA interaction length	mm	1	1
l	bunching drift	mm	2	2,8
δU	Energy spread	keV	7	7

In order to refocus the electrons into the second stage depicted in Fig. 10a, we consider inclusion of a linear focusing field in the drift region between stages. By simple geometrical arguments, we can see that the trace space acceptance for an aperture of width g and length L has the form shown in Fig. 10b. This figure corresponds to the acceptance at the entrance of either structure. After passing through one stage, however, the trace space of a beam having the distribution in Fig. 10b will be inverted in angle (i.e. flipped about the y axis). Consequently in order to match into a subsequent second stage, the intervening focusing should produce a transformation that inverts the trace space in angle but has a point-to-point match in the spatial coordinate. Consider a simple linear focusing field with the transfer matrix

$$M = \begin{bmatrix} \cos Tz & \frac{1}{T}\sin Tz \\ -T\sin Tz & \cos Tz \end{bmatrix} \tag{15}$$

where

$$\begin{bmatrix} y \\ y' \end{bmatrix} = M \begin{bmatrix} y_0 \\ y'_0 \end{bmatrix} \tag{16}$$

We thus want the corresponding relation across the drift region of length l to satisfy $y = y_0$ and $y' = -y'_0$. The resulting relations reduce to a single transcendental equation which we may cast in the form

$$\cos Z + \frac{2}{\nu}\frac{\sin Z}{Z} = 1 \tag{17}$$

with the variable substitution $Z \equiv Tl$ and $\nu \equiv L/l$. The numerical solution to Eq. 17 is plotted in Fig. 11a. For the parameters of Table 5, we have that ν=0.5, Z=2.153 (denoted by blue dot in Fig. 4(a)). We thus obtain $T = 1076m^{-1}$ or $T^2 = 1.16\times10^6 m^{-2}$.

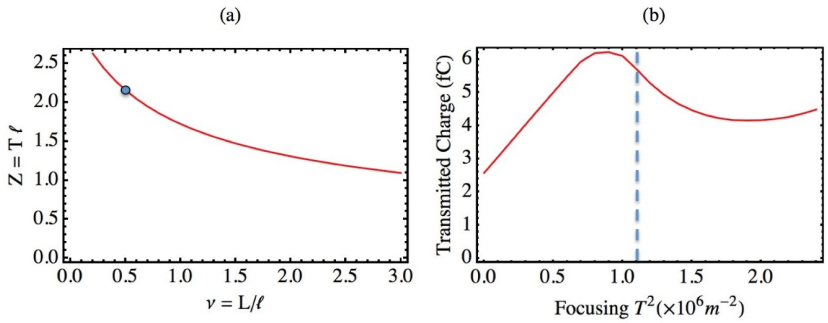

Figure 11: Plots showing (a) the numerical solution to Eq. 17 and (b) the simulated charge transmission for the parameters of Table 5 as a function of focusing strength. The dot on part (a) represents the operating point for the predicted optimal focusing denoted in (b) by a vertical dashed line. The peak transmission is observed to occur close to this estimated value.

We numerically propagated a gaussian beam using the particle tracking code ELEGANT [36] through the configuration of Table 5, modelled as simple apertures with a linear focusing field of the form in Eq. 15 in the 2 mm drift region. The effects of acceleration were not included, as the purpose here was simply to determine the optimal focusing to re-match the transmission from the first DLA stage into the second one. The number of particles in the simulation was 1.86 $\times10^6$ corresponding to an initial bunch charge of Q=300 fC. For a single aperture, the observed transmission was 2.2 %. When combined with a second identical aperture and a focusing field of strength T^2, we obtain the transmitted charge shown in Fig. 11b. We observe that the peak transmission occurs at a value of $T^2 \simeq 0.9 \times 10^6 m^{-2}$. This is remarkably consistent with the value of 1.16 $\times10^6 m^{-2}$ predicted from Eq. 17, which was based only on simple geometrical arguments. We further note that the peak charge transmission of 6 fC corresponds to 2% of the initial 300 fC. Since only 2.2 % of the charge was observed to transmit through a single aperture, this means that almost all of the transmitted charge from the first stage is re-coupled through the second stage. For the beam parameters considered here, this peak focusing field corresponds to a quadrupole gradient of B'=12 kT/m. This is an exceptionally high gradient, exceeding what has been achieved with permanent magnet quadrupoles. It is, however, an order of magnitude less than the estimate of Soong for the Plettner-style dual-grating laser-driven focusing scheme of Refs. [26, 27].

We note also that this value represents the focusing required for an ideal trace space match across the drift between stages in accordance with Eq. 17. Consequently, it is independent of the beam emittance. However, by using a lower emittance beam, the focusing required to achieve a suitable equilibrium beam radius may be substantially reduced, as indicated in Fig. 2b, allowing for improved particle transport through longer devices. Note that for the flat-beam transform emittance and spot sizes indicated in Case 2 of Table 5, the equilibrium vertical focusing condition yields $T^2 = (\epsilon_{Ny}/\beta\gamma\sigma^2)^2 = 5.3 \times 10^4 m^{-2}$, which corresponds to a more readily achievable PMQ gradient of B'=700 T/m. In Fig. 12, transmitted charge for the 50 fC beam of Table 5, Case 2 is shown versus aperture size g with a focusing strength of this magnitude both included and not included (red vs. blue curves) and for two different drift lengths (solid vs. dashed). From these results we see that even with no focusing employed, for our nominal beam aperture of g=1 μm, (corresponding to λ=2 μm) and drift l=2 mm, similar total charge transmission (6 fC) is obtained to that of Case 1 in Fig. 11b). This suggests that for these small beam emittances, external focusing may not be needed to obtain adequate charge transmission for the experimental scenario of Fig. 10. However, the longer drift scenario (l=8 mm) in Fig. 12, illustrates that there is a more substantial degradation in the particle transmission with the PMQs turned off, emphasizing the increased need for external focusing as we move toward longer structures with more stages and/or drift lengths between stages.

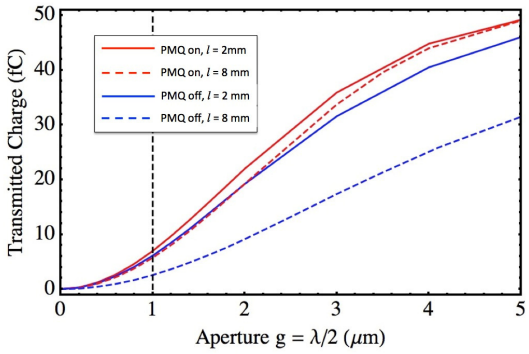

Figure 12: Plots of charge transmission for Case 2 of Table 5 with 50 fC initial bunch charge as a function of the aperture size g with PMQs on and off (at B = 700 T/m) and with two different drift lengths. The Table 5 nominal aperture value (g=1 μm) is shown by a vertical dashed line.

It should also be noted that the accelerating and deflecting fields in the DLA were not included in this tracking simulation. We also have not considered here the dynamics in the orthogonal plane (x). Since the dual-grating structure has a narrow aperture only in the vertical direction, it is more forgiving of larger beam size in x, making it amenable to a flat-beam scenario. A more complete study of the experimental scenario of Fig. 10 that includes the longitudinal and transverse fields and models the microbunching of the beam will be the subject of future work.

7. Conclusions

The use of the flat beam transform to generate strongly asymmetric beams for slab-symmetry DLA structures has been discussed. This technique permits to satisfy the tight demands imposed by the small apertures of these devices using flat photocathodes which allow much larger beam charges than tip-based sources.

Two different cases have been discussed and the implementation of an FBT beamline at the UCLA Pegasus beamline for a two stage DLA experiment is discussed.

The engineering of the magnetic field on the cathode requires further development. One interesting possibility could be to insert a permanent magnet disk just behind the cathode. The field in this case can easily be larger than 0.4 T, but the main problem is the lack of flexibility. Another option would be a large backing solenoid around the rear section of the gun. In this case fields up to 0.15 T can be reached.

Other applications of flat beam include FEL with asymmetric emittances. These have not been studied in detail so far. Further it is also possible to exchange the large emittance with the very small longitudinal emittance in an emittance exchange beamline. This would allow the generation of a beam with ultralow transverse emittance at the expense of poorer quality longitudinal phase space. Considering that laser heaters [37] currently are used to worsen the longitudinal emittances, this might be a path to very compact and efficient FELs.

8. ACKNOWLEDGEMENTS

This work has been partially supported by NSF award 145583 and by the Gordon and Betty Moore Foundation under grant GBMF4744. RJE and KPW acknowledge support of NSF grant number 1535711 and U.S. Department of Energy grant DE-AC02-76SF00515, DE-FG02-13ER41970 and Gordon and Betty Moore Foundation under grant GBMF4744

[1] E. A. Peralta, K. Soong, R. J. England, E. R. Colby, Z. Wu, B. Montazeri, C. McGuinness, J. McNeur, K. J. Leedle, D. Walz, E. B. Sozer, B. Cowan, B. Schwartz, G. Travish, and R. L. Byer. Nature 503, 91 (2013).

[2] J. Breuer and P. Hommelhoff, Phys. Rev. Lett. 111, 134803 (2013).

[3] R. J. England et al. Rev. Mod. Phys. 86, 1337 (2014).

[4] A. Feist, K. E. Echternkamp, J. Schauss, S. V. Yalunin, S. Schfes, C. Ropers, Nature 521, 200 (2015)

[5] D. Ehberger, J. Hammer, M. Eisele, M. Krger, J. Noe, A. Hgele, and P. Hommelhoff Phys. Rev. Lett. 114, 227601 (2015)

[6] D. Cesar, J. Maxson, P. Musumeci, Y. Sun, J. Harrison, P. Frigola, F. H. O'Shea, H. To, D. Alesini, and R. K. Li Phys. Rev. Lett. 117, 024801 (2016)

[7] R. Brinkmann, Y. Derbenev and K. Floettmann. Phys. Rev. ST Accel. Beams 4, 053501 (2001)

[8] Y.-E. Sun, P. Piot, K.-J. Kim, N. Barov, S. Lidia, J. Santucci, R. Tikhoplav, and J. Wennerberg, Phys. Rev. ST Accel. Beams 7, 123501 (2004).

[9] P. Piot, Y.-E. Sun, and K.-J. Kim, Phys. Rev. ST Accel. Beams 9, 031001 (2006).

[10] A. Valloni, A. Cahill, A. Fukasawa, P. Musumeci, B. Spataro, A. Yakub, and J. B. Rosenzweig, AIP Conf. Proc. 1507, 762 (2012).

[11] D. Cesar et al. to be submitted

[12] J. B. Rosenzweig et al. arxiv.org/pdf/1603.01657 (2016)

[13] Physics Procedia, 52, 2 (2014)

[14] these proceedings.

[15] L. Schachter, W. D. Kimura, and I. Ben-Zvi, Ultrashort Microbunch Electron Source, in Proceedings of the Advanced Accelerator Concepts Workshop, San Jose, CA (2014).

[16] C. M. S. Sears, et al., Phys. Rev. ST Accel. Beams 11, 101301 (2008).

[17] C. M. S. Sears, et al., Phys. Rev. ST Accel. Beams 11, 061301 (2008).

[18] R. H. Siemann, Phys. Rev. ST Accel. Beams 7, 061303 (2004).

[19] Y. C. Neil Na, R. H. Siemann and R. L. Byer, Phys. Rev. ST Accel. Beams 8, 031301 (2005).

[20] Helfenstein, P., et al., Appl. Phys. Lett. 98, 061502 (2011).

[21] Mustonen, A., P. Beaud, E. Kirk, T. Feurer, and J. L. Shaw, 2011, Appl. Phys. Lett. 99, 103504.

[22] M. Szilagyi, Electron and Ion Optics, p.161, Plenum Press, NY (1988).

[23] P. Grivet, Electron Optics, 2nd Ed., p. 36, Pergamon Press, Oxford (1972).

[24] H. Bartzsch, et al., Phys. Status Soldi A 206 (3), 514 (2009)

[25] J. Szmidt, Surface Coatings and Tech. 47, 496 (1991).

[26] K. Soong, et al., Grating-based deflecting, focusing, and diagnostic dielectric laser accelerator structures, AIP Conf. Proc. 1507, 516 (2012).

[27] Plettner, T., R. L. Byer, and B. Montazeri, J. Mod. Opt. 58, 1518 (2011).

[28] Ivan V. Bazarov, Bruce M. Dunham, and Charles K. Sinclair Phys. Rev. Lett. 102, 104801 (2009)

[29] L. Cultrera, S. Karkare, H. Lee, X. Liu, I. Bazarov, and B. Dunham Phys. Rev. ST Accel. Beams 18, 113401 (2015)

[30] Marta Csatari Divall, Eduard Prat, Simona Bettoni, Carlo Vicario, Alexandre Trisorio, Thomas Schietinger, and Christoph P. Hauri Phys. Rev. ST Accel. Beams 18, 033401 (2015)

[31] P Musumeci, JT Moody, CM Scoby, MS Gutierrez, M Westfall, RK Li Journal of Applied Physics 108 (11), 114513 (2010)

[32] K.-J. Kim and V. Kumar. Phys. Rev. ST Accel. Beams 10, 080702 (2007).

[33] Y.-E Sun, phD Thesis University of Chicago (2005)

[34] R. K. Li, K. G. Roberts, C. M. Scoby, H. To, and P. Musumeci Phys. Rev. ST Accel. Beams 15, 090702 (2012)

[35] K. P. Wootton, et al., "Demonstration of acceleration of electrons at a dielectric microstructure using femtosecond laser pulses," Optics Letters 41 (12), 2672 (2016).

[36] M. Borland, "ELEGANT: A Flexible SDDS-Compliant Code for Accelerator Simulation," Advanced Photon Source LS-287, September 2000.

[37] Z. Huang, A. Brachmann, F.-J. Decker, Y. Ding, D. Dowell, P. Emma, J. Frisch, S. Gilevich, G. Hays, Ph. Hering, R. Iverson, H. Loos, A. Miahnahri, H.-D. Nuhn, D. Ratner, G. Stupakov, J. Turner, J. Welch, W. White, J. Wu, and D. Xiang. Phys. Rev. ST Accel. Beams 13, 020703 (2010)